Treg-selective IL-2 starvation synergizes with CD40 activation to sustain durable responses in lymphoma models

Kristin Stirm [1], Peter Leary,[1] Daria Wüst,[1] Dominique Stark [1], Nicole Joller,[2] Ufuk Karakus,[3] Onur Boyman,[3,4,5] Alexandar Tzankov,[6] Anne Müller [1,4]

[1]Institute of Molecular Cancer Research, University of Zurich, Zurich, Switzerland
[2]Department of Quantitative Biomedicine, University of Zurich, Zurich, Switzerland
[3]Department of Immunology, University Hospital Zurich and University of Zurich, Zurich, Switzerland
[4]Comprehensive Cancer Center Zurich, Zurich, Switzerland
[5]Faculty of Medicine, University of Zurich, Zurich, Switzerland
[6]Institute of Medical Genetics and Pathology, University Hospital Basel and University of Basel, Basel, Switzerland

Correspondence to
Dr Anne Müller;
mueller@imcr.uzh.ch

ABSTRACT

Background Roughly half of all diffuse large B-cell lymphomas (DLBCLs) are infiltrated by large numbers of regulatory T-cells (Tregs). Although the presence of 'effector' Tregs in particular is associated with an inferior prognosis in patients on standard rituximab plus cyclophosphamide, doxorubicin, vincristine, and prednisone (R-CHOP) immunochemotherapy, the role of this cell type during lymphoma initiation and progression is poorly understood.

Methods Here, we use tissue microarrays containing prospectively collected DLBCL patient specimens, as well as data from publicly available cohorts to explore the mutational landscape of Treg-infiltrated DLBCL. We further take advantage of a model of MYC-driven lymphoma to mechanistically dissect the contribution of Tregs to lymphoma pathogenesis and to develop a strategy of Treg-selective interleukin-2 (IL-2) starvation to improve immune control of MYC-driven lymphoma.

Results We find that all genetic DLBCL subtypes, except for one characterized by co-occurring *MYD88/CD79* mutations, are heavily infiltrated by Tregs. Spectral flow cytometry and scRNA-sequencing reveal the robust expression of functional and immunosuppressive markers on Tregs infiltrating MYC-driven lymphomas; notably, we find that intratumoral Tregs arise due to local conversion from naïve CD4^{+} precursors on tumor contact. Treg ablation in Foxp3[iDTR] mice, or by antibody-mediated Treg-selective blockade of IL-2 signaling, strongly reduces the lymphoma burden. We identify lymphoma B-cells as a major source of IL-2, and show that the effects of Treg depletion are reversed by the simultaneous depletion of Foxp3-negative CD4^{+} T-cells, but not CD8^{+} T-cells or natural killer (NK) cells. The inhibition of ATP hydrolyzation and adenosine production by Tregs at least partly phenocopies the effects of Treg depletion. Treg depletion further synergizes with pro-apoptotic CD40 activation to sustain durable responses.

Conclusion The combined data implicate Tregs as a potential therapeutic target in DLBCL, especially in combination with other immunotherapies.

WHAT IS ALREADY KNOWN ON THIS TOPIC

⇒ Regulatory T-cells (Tregs) are known to infiltrate lymphomas of the diffuse large B-cell (DLBCL) type, but their role in lymphoma growth and progression has not been studied in experimental models, and the prognostic significance of Treg infiltration is controversial.

WHAT THIS STUDY ADDS

⇒ We show here that Tregs infiltrating an experimental, MYC-driven lymphoma have characteristics of 'effector' Tregs and differ strongly from their normal thymus-derived counterparts in terms of their immunophenotype and transcriptome.

⇒ The depletion of Tregs, either in a genetic model or by interleukin-2 (IL-2) starvation, strongly reduces the lymphoma burden, especially when combined with treatments that directly compromise tumor cell viability.

HOW THIS STUDY MIGHT AFFECT RESEARCH, PRACTICE OR POLICY

⇒ Our study implies that DLBCL that is refractory to standard of care treatments, but infiltrated by large numbers of Tregs, might benefit from experimental Treg-directed therapy, in particular starvation with a Treg-selective IL-2-targeting antibody that is currently in clinical development.

INTRODUCTION

Diffuse large B-cell lymphoma (DLBCL) is an aggressive, highly heterogeneous malignancy derived from mature B-cells that is fatal in a third of patients. The two major advances in DLBCL treatment were the addition of the CD20-specific antibody rituximab to standard chemotherapy two decades ago[1 2] and the recent approval of chimeric antigen receptor (CAR) T-cell therapy for a select group of patients with DLBCL.[3] DLBCL originates from antigen-exposed B-cells that have undergone the germinal center (GC) reaction.[4] Several molecular subtypes can be distinguished based on transcriptional and mutational signatures, copy number alterations and structural variants.[5 6] One of the hallmarks of DLBCL arising in immunocompetent patients—in contrast to post-transplant patients on immunosuppressive therapy[7]—is the mutational inactivation of various genes associated with

immune detection and surveillance. Examples include the genes encoding β2-microglobulin and CD58, which are required for cytotoxic T-cell and natural killer (NK) cell recognition and killing of DLBCL cells; both genes are recurrently targeted by deletions, frameshift and other inactivating mutations and their surface expression is compromised in >60% of DLBCL cases.[8] Although not directly targeted by mutations, *MHCII* gene expression is abrogated in DLBCL harboring inactivating mutations in the genes encoding the histone acetyltransferases (HATs) CREB binding protein (CREBBP) and EP300; such mutations occur in 30% of DLBCL[9] and prevent surface MHCII expression and detection by CD4$^+$ T-cells through loss of the active (acetylated) histone mark on H3K14, H3K18, and H3K27.[10–12] Various genetic aberrations lead to programmed death-ligand 1 (PD-L1) overexpression in one-third of DLBCL cases; these include gene amplifications, transcript stabilization by truncation of the 3′-UTR and translocations of *IGH, PIM1,* and *TP63* to the *PDL1* locus.[13 14] However, the clinical relevance of PD-L1 overexpression in DLBCL is not clear and trials of PD-1/PD-L1 blockade in DLBCL have delivered variable results, both as frontline therapy in combination with rituximab plus cyclophosphamide, doxorubicin, vincristine, and prednisone (R-CHOP) in PD-L1 positive patients and as salvage therapy in the setting of relapse after CART19/20 therapy.[15–18] The lymphoma microenvironment of DLBCL has recently received increasing attention as a result of the availability of fluorescent multiplex immunohistochemistry (IHC) and automated quantification technologies, and certain microenvironmental features appear to predict the outcome of patients under R-CHOP therapy.[19–21]

We focus here on regulatory T-cells (Tregs) as highly variable, possibly predictive and targetable components of the lymphoma microenvironment. The prognostic value of Treg infiltration varies with the cell of origin DLBCL subtype[22] and depends strongly on whether all CD25$^+$ Foxp3$^+$ Tregs, or only 'effector' Treg subpopulations were considered in the respective study.[23–26] While strong Treg infiltration of the 'activated B-cell' (ABC) and 'not otherwise specified' (NOS) DLBCL subtypes is negatively prognostic, the opposite is true for Treg infiltration of the 'germinal center B-cell' (GCB) DLBCL subtype.[22] The presence of Foxp3$^+$ Tregs not further subclassified by additional markers is mostly considered to be beneficial[23 25]; in contrast, the infiltration of 'effector' regulatory T-cells, coexpressing inhibitory markers such as cytotoxic T-lymphocyte-associated protein 4 (CTLA-4) or T-cell immunoglobulin and mucin domain 3 (TIM-3) along with Foxp3, is usually associated with a poor prognosis,[24 26] as is a high Treg count in the blood of patients with DLBCL.[27] We have previously shown that DLBCL arising on a background of immunosuppression due to solid organ transplantation are generally devoid of Treg infiltration[28] and also lack many of the above-mentioned genetic adaptations of immune escape, such as immune-evasive *B2M* mutations.[7] We demonstrate here that Tregs form an integral part of the lymphoma microenvironment not only in human DLBCL but also in a MYC-driven serial transplantation model of the disease, where up to 80% of intratumoral CD4$^+$ T-cells are Foxp3$^+$ Tregs. Intratumoral Tregs differ radically from their normal counterparts in non-tumor-bearing lymph nodes with respect to their immunophenotype and gene expression profile. The selective ablation of Tregs by diphtheria toxin in Foxp3^{iDTR} mice abrogates lymphoma growth, which can be recapitulated by selective starvation of Tregs of their growth factor IL-2. Lymphoma cells are capable of locally converting naïve T-cells into Tregs. Intratumoral Tregs act already at the earliest stages of lymphomagenesis in our experimental model, and serve to locally suppress CD4$^+$ but not CD8$^+$ effector T-cell or NK cell responses.

METHODS
Animal experimentation and tissue processing

For the syngeneic serial transplantation model of MYC-overexpressing lymphoma cells, 1×10^6 cryopreserved splenic tumor cells in 100 µL phosphate buffered saline (PBS) were injected intravenously into 6–8 weeks old mixed-gender mice. Anti-mouse CD8 (clone YTS 169.4; isotype: rat IgG2b), anti-mouse CD4 (clone YTS 191; rat IgG2b), anti-mouse NK1.1 (clone PK136; mouse IgG2a), anti-mouse CD25 (clone PC-61.5.3; rat IgG1), anti-mouse CD73 (clone TY/23; rat IgG2a), anti-mouse TIM3 (clone B8.2C12; rat IgG1), anti-mouse CTLA-4 (clone 9H10; Syrian hamster IgG), anti-mouse GITR agonist (clone DTA-1; rat IgG2b), anti-mouse PD-L1 (clone 10F.9G2; rat IgG2b), anti-mouse CD40 agonist (clone FGK4.5; rat IgG2a), anti-horseradish peroxidase isotype control (clone HRPN; rat IgG1), and anti-keyhole limpet hemocyanin isotype control (clone LTF-2; rat IgG2b) antibodies were purchased from BioXCell. Anti-mouse TIGIT (clone 1B4; mouse IgG1)[29] and anti-mouse IL-2 (clone NARA-1; rat IgG2a)[30] antibodies were recently described. Mice were administered an initial 300 µg dose intraperitoneally on the day of tumor cell injection, followed by 200 µg injections every fourth day until the study endpoint (day 10–11), unless otherwise specified. Anti-TIGIT and anti-CD40 were administered at 100 µg doses and anti-IL-2 at 50 µg or 100 µg doses. Mice were monitored during the course of the experiment for symptoms of disease including enlarged lymph nodes (LNs), weight loss and hind leg paralysis, which were all criteria for study termination. B6.129(Cg)-Foxp3tm3(DTR/GFP)Ayr/J mice used for the serial transplantation model were depleted of Tregs by intraperitoneal injections of 20 ng/g diphtheria toxin from corynebacterium (Sigma Aldrich, D0664), diluted in 100 µL sterile PBS at the day of tumor cell inoculation and repeated every third day until study endpoint, if not otherwise stated. The mouse strains B6.129(Cg)-Foxp3tm3(DTR/GFP)Ayr/J, B6.129(Cg)-Foxp3tm4(YFP/icre)Ayr/J, B6.Cg-Tg(IghMyc)22Bri/J and B6-Tg(TcraTcrb)425Cbn/J x B6.SJL-Ptprc^a Pepc^b/BoyJ were obtained from the Jackson Laboratories.

Diseased mice were euthanized, and their spleens and inguinal and axillary LNs were weighed. Spleens and axillary plus inguinal LNs were passed through a 40 µM cell strainer to produce single-cell suspensions. Cells isolated from spleens, femoral bone marrow and peripheral blood were treated with ACK red blood cell lysis buffer pH 7.2–7.4 (150 mM NH_4Cl, 10 mM $KHCO_3$, 0.1 mM Na_2EDTA). T cells of single-cell suspensions were subjected to PMA/ionomycin restimulation for 3 hours, followed by intracellular cytokine staining. Mice were injected intraperitoneally with 20 µg Fingolimod (FTY720, Sigma Aldrich, reconstituted in dimethyl sulfoxide (DMSO)), diluted in 0.9% saline, pH 7.4. Control mice were injected with DMSO diluted in 0.9% saline, pH 7.4. Fingolimod was injected daily starting 1 day before tumor cell inoculation and continued every second day until study endpoint. All animal studies were reviewed and approved by the Zurich Cantonal Veterinary Office (licenses 132/2019 and 007/2022 and their amendments, to AM).

Flow cytometric analysis

Cells were stained with the following fluorescently labeled mouse-specific antibodies and used at 1:200 dilution for extracellular staining and at 1:100 dilution for intracellular staining: BV650 CD45 (BioLegend, 30-F11), BV510 TCR (BioLegend, H57-597), BV711 (BioLegend, RM4-5), BUV496 CD4 (BD Bioscience, GK1.5), AF700 CD8 (BioLegend, 53-6.7), PE-Cy7 IFNγ (BioLegend, XMG1.2), PerCp-Cy5.5 IL10 (BioLegend, JES5-16E3), PE-Cy5 CD19 (eBioscience, eBio1D3), BV785 NK1.1 (BioLegend, PK136), FITCb NK1.1 (BioLegend, PK136), FITC IL2 (BioLegend, JES6-5H4), BUV395 CD45 (BD Biosciences, 30-F11), AlexaFluor700 CD8a (BioLegend, 53-6.7), BV570 CD62L (BioLegend, MEL-14), BV605 CTLA4 (BioLegend, UC10-4B9), BV421 Neuropilin-1 (BioLegend, 3E12), BUV737 CD44 (BD Biosciences, IM7), BV480 Ki67 (BD Biosciences, B56), FITC FoxP3 (eBioscience, FJK-16s), BV650 CD25 (BioLegend, PC61), BUV805 CD27 (BD Biosciences, LG.3A10), BV711 PD-1 (BioLegend, 29F.1A12), PB CD73 (BioLegend, TY/11.8), PerCP-Cy5.5 GITR (BioLegend, DTA-1), BUV661 GITR (BD Biosciences, DTA-1), PerCP-eFluor710 CD39 (eBioscience, eBioA1), PE TIM3 (R&D Systems, #215008), APC LAG3 (BioLegend, C9B7W), BV750 ICOS (BioLegend, C398.4A), PE-Dazzle594 TIGIT (BioLegend, 1G9), PE-Cy7 Tbet (BioLegend, 4B10), AlexaFluor647 Tbet (BioLegend, 4B10), PE-Cy7 Fas/CD95 (BD Biosciences, Jo2), APC FasL (BioLegend, MFL3), PerCP-Cy5.5 CD40 (BioLegend, 3/23), APC FasL (BioLegend, MR1), BV785 CD69 (BioLegend, H1.2F3), PE-eFluor610 RORγt (eBioscience, B2D), BV786 CD119/IFNGR1 (BD Biosciences, GR20), eFluor660 TOX (eBioscience, TXRX10), purified CD16/32 (93, 1:100), and Fixable Viability Dye eFluor 780 eBio/Affymetrix (1:1000). For intracellular staining of transcription factors, cells were fixed using the eBioscience fixation/permeabilization kit (Invitrogen, 00-5223-56, 00-5123-43), whereas for intracellular cytokine staining, cells were fixed using the BD cytofix/cytoperm kit (BD Bioscience, 554714). Apoptotic cells were detected by AnnexinV-PE-Cy7 staining (BioLegend, 640951). For high dimensional flow cytometric analysis, data were acquired on a Cytek Aurora, or on a Symphony (BD) flow cytometer and analyzed with the FlowJo software package (TreeStar). FCS files of gated cells of interest were exported from FlowJo and imported into R using the 'flowCore' R Bioconductor package V.2.8.0 and down-sampled to 1000 cells per sample. Cofactors for hyperbolic arcsine transformation were determined using the Cytobank Community edition web platform (Kotecha et al, 2010[31]). Imported FCS files were integrated into a SingleCellExperiment object and arcsine transformed using the CATALYST R Bioconductor package V.1.20.1 (https://github.com/HelenaLC/CATALYST). Dimensionality reduction was performed using CATALYST. Cell clusters were identified using an R-based implementation of the PhenoGraph algorithm (https://github.com/JinmiaoChenLab/Rphenograph).[32] Pairwise differential abundance of cell clusters between conditions was performed using the edgeR method, and differential state between clusters within conditions and across conditions using the limma method, in the 'diffcyt' R Bioconductor package V.1.16.0 (github.com/lmweber/diffcyt). All R functions were executed on R V.4.2 (R Core Team, 2020) and Bioconductor V.3.15.

ScRNA-Seq and TCGA RNA-Seq analysis

Axillary and inguinal LNs of 3–4 tumor-bearing and non-tumor-bearing FoxP3[cre]-YFP mice, respectively, were isolated as described above. Single cell suspensions were stained with the following antibodies for Treg sorting on the BD FACS Aria III (BD Biosciences, Switzerland): PB CD45 (BioLegend, 30-F11), PerCP-Cy5.5 CD4 (BioLegend, RM4-4), fixable viability dye eFluor780 (eBioscience) and anti-mouse CD16/32 (BioLegend, 98). About 100,000 live $CD4^+$ $FoxP3/YFP^+$ Tregs per sample were sorted and collected in IMDM (Gibco, 12440-053) containing 20% FCS (Gibco, 10270-106) and 1% PenStrep (Gibco, 15140-122). After cell sorting, cells were resuspended in 50 µL $MgCl_2$ and $CaCl_2$ free 1X PBS (Gibco, 10010-015) and incubated with 0.5 µL anti-mouse CD16/32 for 10 min on ice. For hash-tagging, cells were incubated with 1.5 µg TotalSeqTM-C0301 anti-mouse Hashtag 1 (BioLegend, M1/42, 30-F11) and TotalSeqTM-C0302 anti-mouse Hashtag 2 (BioLegend, M1/42, 30-F11), respectively, for 30 min on ice. Samples were washed three times with 3.5 mL $MgCl_2$ and $CaCl_2$ free PBS and subjected to scRNA-Seq at the Functional Genomics Center Zürich. Samples were prepared for sequencing using the 10X Genomics BCR/TCR (VDJ) with Feature Barcoding Single Cell reagent kit, following manufacturer's protocol. Sequencing was performed on the Illumina NovaSeq 6000. Demultiplexing was performed using the Illumina bcl2fastq Conversion Software. Gene expression sequencing generated 351 million reads, VDJ sequencing 20 million reads, and Feature Barcode sequencing 66 million reads. Initial analysis of scRNA-Seq data was

performed using the SUSHI framework which encompassed the following steps: Read quality was inspected using FastQC (http://www.bioinformatics.babraham.ac.uk/projects/fastqc/); cell identification, read mapping and gene quantification, and sample demultiplexing was performed using 10X Genomics Cell Ranger V.6.0.2 with the GENCODE mouse genome build GRCm39 release M26[33]; cell clonotypes were identified using cellRanger's 'vdj' function, and the Seurat V.4.1.1.9003[34] Bioconductor R package was used to demultiplex the cells, identify cell doublets and dropouts based on hashtags, normalize the gene expression counts (log normalize, scale factor of 10,000), find variable genes (vst, 3000 genes), scale and center the dataset, variance-transform the counts using 'SCTransform', run PCA, TSNE and UMAP dimensional reduction (1–20 dimensions), find neighbors (pca, 1–20 dimensions) and clusters (multiple resolutions from 0.2 to 1, with 0.6 the resolution used), and find all marker genes for each cluster (Wilcox). The code used for these steps is available on the 'ezRun' Github page (https://github.com/uzh/ezRun/blob/master/R/app-SCFeatBarcoding.R). VDJ-based cell clonotype data were integrated into the Seurat object using the 'scRepertoire' R Bioconductor package (www.bioconductor.org/packages/release/bioc/html/scRepertoire.html), and clonotypes were clustered based on TRA amino acid sequence at 80% similarity. All R functions were executed on R V.4.2 (R Core Team, 2020) and Bioconductor V.3.15.

Gene-level counts of 481 samples were downloaded from the TCGA project NCICCR-DLBCL. Counts were generated by the STAR aligner and the human genome build GRCh38.p0. Clinical data associated with each sample were also downloaded from TCGA. Count files were imported into R V.4.0.2 for downstream analysis (including library normalization and transformation) in the DESeq2 package V.1.28.1. Samples that had a genetic subtype of 'other' were excluded from downstream analysis, leaving a final count of 220 samples. The DESeq2 model incorporated only the genetic subtype classification. Variance stabilized transformed counts were used to generate boxplots of target gene expression as a function of genetic subtype. Global and pairwise Kruskal-Wallis one-way analysis of variance (ANOVA) was used to generate p values of expression across and between genetic subtypes. Whole exome sequencing (WXS) BAM files of 472 patients were downloaded from the TCGA project NCICCR-DLBCL. BAM files were generated using the BWA aligner and the human genome build GRCh38.p0, and included marking of duplicate reads and base quality score recalibration following GATK best practice recommendations. On downloading, each BAM file was filtered using a BED file of a 258-gene pane, sorted, and indexed, using SAMtools.[35] This panel was derived from the genes with variants as published.[6] Due to a lack of matched normals, somatic variants were called using Mutect2 from GATK V.4.1.8.0 in tumor-only mode. Variants were then annotated using Funcotator from GATK. MAF files generated from Funcotator were imported into R using the R package Maftools V.2.4.05. Samples with a genetic subtype of 'other' were excluded from downstream analysis,

leaving a final count of 206 samples. Variants that had fewer than 10 reads supporting the variant allele, and variants that had an allele frequency of greater than 2% in the gnomAD exome database, were discarded. Oncoplots, co-oncoplots, and forest plots were generated using the respective Maftools function. For the co-oncoplots, only the 25% of samples with the highest and 25% with the lowest respective gene expression were directly compared.

IHC and immunofluorescence microscopy of DLBCL patient cohorts and murine tissues

The two DLBCL patient cohorts used here are described in Juskevicius *et al*[36] and in the website (https://www.eahp-sh2022.com/wp-content/uploads/2022/09/Lymphoma-symposium.pdf). Tissue microarrays (TMAs) were stained for FoxP3 using the clone SP97 (Abcam, ab99963) at 1:50 dilution and for CD40 using the clone CL1673 (Novus Biological, NBP2-34488) at a 1:800 dilution. Cases containing ≥5% FoxP3+tumor-infiltrating T-cells were considered positive[22] and CD40 was scored as follows: 0, negative; 1, weakly positive in <50% of tumor cells; 2, either weakly positive in >50% or moderately positive in 10%–50% of tumor cells; 3, either moderately positive in >50% or strongly positive in tumor cells. For co-immunofluorescence microscopy, patient cryosections were thawed at room temperature (RT), rehydrated in PBS and incubated in blocking buffer (1:2 PBS, 1:4 normal goat serum (Vector Laboratories, S-1000), 1:4 7.5% bovine serum albumin (BSA) in PBS, 1% ChromePure IgG (Jackson Immunology, 154669)) for 30 min. After washing, the following primary anti-human antibodies (1:100 in blocking solution) were added: rabbit FoxP3 (Sigma-Aldrich, HPA045943), rat Ki67 (Invitrogen, SolA15), and incubated over night at 4°C. Slides were incubated with the following secondary antibodies diluted 1:400 in 7.5% BSA in PBS for 2 hours at RT in the dark: goat anti-rat IgG AlexaFluor488 (Invitrogen, A11006) and goat anti-rabbit IgG AlexaFluor568 (Invitrogen, A11011). After washing, DAPI (Thermo Fisher, 62248, 1:1000 in PBS) was added for 5 min, slides rinsed, dried at RT and 20 μL mounting medium (Invitrogen, Fluoromount-GTM, 00-4958-02) and cover slips (epredia) were added. Images were recorded using a Leica DM6 B Microscope. Informed consent was obtained from all subjects, and all experiments using human material conformed to the principles set out in the WMA Declaration of Helsinki and the Department of Health and Human Services Belmont Report. The Ethics Committee of Northwestern and Central Switzerland and the Ethics Committee of both Basel Cantons approved the work with patient material presented here (EKNZ 2014-25 and 282/08, respectively).

Spleens harvested from tumor-bearing and non-tumor-bearing mice were fixed for 24 hours in 4% PFA (Laborchem international, LC-6470.5) at RT. After paraffin-embedding, tissues were fixed to the slides by baking at 52°C for 3 hours, then dewaxed with Xylol (Sigma-Aldrich, STBJ5892), rehydrated using an ethanol dilution series (100% EtOH, 90% EtOH, 75% EtOH, H_2O, PBS). Slides were subjected to antigen retrieval by boiling for 2 hours in a water bath in 1× citrate buffer (Sigma, C9999-1, 10× stock, pH 6), followed by

blocking in 25% normal goat serum (Vector Laboratories, S-1000), 25% PBS, 25%–7.5% BSA and 1% ChromePure IgG (Jackson Immunology, 154669) for 1 hour. Slides were incubated overnight with the following primary anti-mouse antibodies (1:100 in blocking solution): rabbit FoxP3 (Cell Signaling Technology, D608R) and rat Ki67 (Invitrogen, SolA15). After washing, the following secondary antibodies (1:400 in 7.5% BSA) were added for 2 hours in the dark: goat anti-rat IgG Alexa Fluor 488 (Invitrogen, A11006), goat anti-rabbit IgG Alexa Fluor 568 (Invitrogen, A11011). After washing, DAPI (Thermo Fisher, 62248, 1:1000 in PBS) was added for 5 min, followed by mounting.

Cell culture experimentation

We used a panel of 13 DLBCL cell lines including six of the GCB subtype (SU-DHL4, SU-DHL5, SU-DHL6, SU-DHL8, SU-DHL10, and SU-DHL16), 6 of the ABC subtype (HBL-1, OCI-Ly3, OCI-Ly10, SU-DHL2, RIVA and U-2932) and 1 unclassified DLBCL cell line (RC-K8) that have been previously described.[10 37 38] All cell lines were routinely tested and negative for mycoplasma. Cell line authentication was performed according to the guidelines of the International Cell Line Authentication Committee using short tandem repeat profiling; the result of this effort was described recently for all cell lines used here, along with their sources.[39] Cell lines were maintained at 37°C and 5% CO_2 in IMDM (OCI-Ly3, OCI-Ly10, RIVA) or RPMI (all others) supplemented with 10% (OCI-Ly3, RIVA) or 20% (all others) heat-inactivated fetal calf serum (FCS, Gibco) and 100 U/mL penicillin and 100 µg/mL streptomycin. Primary murine MYC-overexpressing lymphoma cells were cultured in high-glucose Dulbecco's modified Eagle's medium (DMEM) supplemented with 10% FCS, 50 µM β-mercaptoethanol (Sigma-Aldrich), 100 U/mL penicillin, 100 µg/mL streptomycin (Gibco), and 100 µM L-asparagine (Sigma-Aldrich) at 37°C and 10% CO_2.

Quantitative RT-PCR

RNA was extracted using the NucleoSpin RNA kit (Macherey-Nagel) according to the manufacturer's instructions. One microgram of total RNA was reverse-transcribed using SuperScript III reverse transcriptase (Invitrogen). TaqMan gene expression assays (Thermo Fisher Scientific) were performed for the following genes: human CD40 (Hs00386848_m1), human IL-2 (Hs00174114_m1) and human ACTB (HS01060665_g1). The samples were analyzed on a LightCycler 480 instrument (Roche) and target mRNA abundance was calculated relative to ACTB.

Statistics

All statistical analyses were performed using GraphPad Prism software. Graphs represent means plus SD of at least two independent experiments. Statistical analysis was performed using ordinary one-way ANOVA in case of three or more groups or unpaired two-tailed Mann-Whitney test for a comparison of two groups.

RESULTS

MYC-expressing lymphomas are infiltrated by large numbers of activated Tregs that express high levels of immunosuppressive markers

To characterize the Tregs infiltrating the lymphoma microenvironment in a convenient, rapid and standardized model, we took advantage of MYC-expressing lymphoma cells from Eμ-MYC mice, which, on transplantation into syngeneic immunocompetent C57BL/6 recipients, form tumors in the LNs, spleen and bone marrow within 10–12 days post-transplant; tumor cells can be readily identified flow cytometrically by their CD19, intermediate CD45 and Ki67 expression.[28] MYC-driven lymphomas in the LNs (and spleens, data not shown) are highly enriched for Foxp3+ Tregs relative to control LNs (figure 1A). The extent of Treg infiltration correlates strongly with the tumor burden (figure 1B). Tregs infiltrate the tumor mass and are found in close proximity to tumor B-cells (figure 1C). Spectral flow cytometry using a panel of 14 antibodies specific for relevant Treg markers identified five Treg clusters that were predominantly found in normal LNs and consisted of naïve cells (CD62L+, CD44-) with low to intermediate expression of functional/immunosuppressive markers (CD39, CD73, GITR) (figure 1D–G, online supplemental figure S1A,B); the immunophenotype of normal LN Tregs described here is consistent with the published markers of thymus-derived Tregs in murine secondary lymphoid organs.[40] In contrast, Tregs within tumors showed downregulation of CD62L and enhanced expression of the immunosuppressive markers CD39, CD73 and GITR, of neuropilin-1 (Nrp-1) and of the interleukin-2 (IL-2) receptor α-subunit CD25 (figure 1D–G, online supplemental figure S1B), all of which are attributes of effector Tregs.[41] The largest changes in the expression between control and tumor-infiltrating Tregs were observed in CD62L, Nrp-1, CD25 and CD73/CD39, two enzymes that convert immunostimulatory ATP into immunosuppressive adenosine (online supplemental figure S1B). Only one, numerically minor cluster of (tumor-infiltrating) Tregs was positive for Ki67, indicating active proliferation (figure 1G). Tumor-infiltrating Tregs appeared in tumors of wild-type as well as T-cell-receptor (TCR)-transgenic OTII recipients, in which the TCRs of all CD4+ T-cells, including Tregs, are specific for the chicken ovalbumin peptide 323–339; this result indicates that Treg recruitment and/or local expansion is not dependent on binding to cognate antigen (figure 1H). Regular orally administered doses of the sphingosine-1-phosphate analog fingolimod, which prevents lymphocyte egress from lymphoid tissues, did not prevent the appearance of effector Tregs within the transplanted lymphoma, indicating that these cells arise as a consequence of local differentiation or expansion, rather than recruitment from the circulation or from distant lymphoid organs (figure 1I). Indeed, the adoptive transfer of >95% pure, Foxp3/YFP-, naïve CD45.2+ CD4+ T-cells sorted from Foxp3^YFP reporter mice into tumor-bearing CD45.1+ congenic recipients led to their efficient
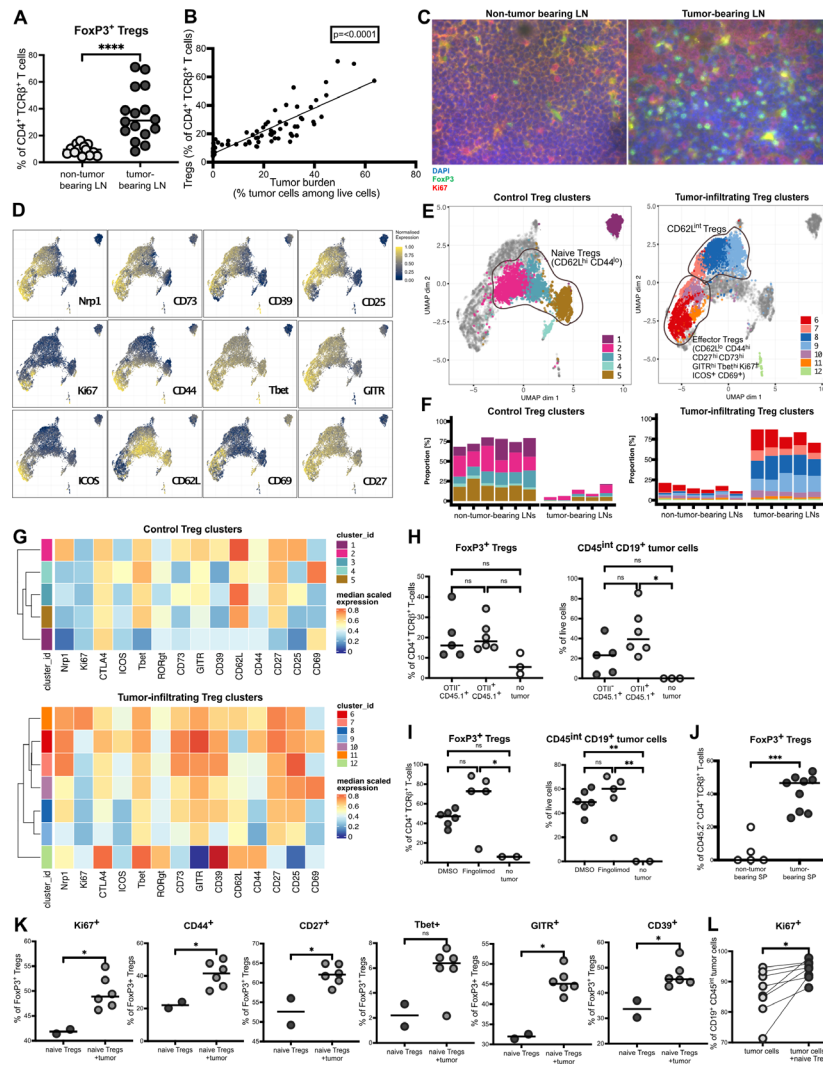
Figure 1 Regulatory T-cells (Tregs) in MYC-driven lymphomas differ immunophenotypically from normal lymph node (LN) Tregs. (A–G) C57BL/6 mice were intravenously injected with 1 Mio >90% pure lymphoma cells isolated from the spleens of Eμ-Myc-transgenic donors; frequencies of tumor cells and Tregs in pooled axillary and inguinal LN preparations were determined by flow cytometry at the study endpoint (A, B; 10–11 days post injection). Ki67+ tumor B-cells and Foxp3+ Tregs were visualized by immunofluorescence microscopy (C; scale bar: 50 mm). A subset of mice was subjected to multidimensional flow cytometry using a panel of 14 intracellular and surface markers that allowed the identification and quantification of the 12 indicated naïve and effector Treg populations. Individual marker UMAPs ("uniform manifold approximation and projection") are shown in (D) and UMAPs showing the FlowSOM-guided manual metaclustering of the 12 indicated control and tumor-infiltrating Treg clusters is shown for six control and five tumor-bearing mice in (E) alongside their quantification in (F). Naïve, transitional CD62L^{int} and effector Tregs are indicated. The heatmaps in (G) show the median expression of the indicated markers (value range: 0–1) of control and tumor-infiltrating Treg clusters. Data in (A) and (B) are pooled from three studies; data in (D)–(G) are from one study, and representative of at least three independently conducted studies. (H) CD45.1+ (Ly5.1+) OTII-TCR-transgenic (OTII+) and their WT (OTII-) littermates were intravenously injected with 1 Mio MYC-expressing lymphoma cells and frequencies of Tregs and tumor B-cells were determined in LN single cell suspensions by flow cytometry at the study endpoint. (I) C57BL/6 mice were injected with 1 Mio splenic MYC-overexpressing lymphoma cells and treated intraperitoneally every second day with 20 μg fingolimod or the diluent dimethyl sulfoxide (DMSO) only, starting 1 day before tumor cell inoculation. Frequencies of Tregs and tumor cells were determined by flow cytometry at the study endpoint. (J) CD45.1+ (Ly5.1+) tumor-bearing or non-tumor-bearing mice were adoptively transplanted with 1 Mio sorted CD45.2+ FoxP3/YFP- CD4+ T-cells on day 9 post tumor cell transplantation; the frequencies of converted CD45.2+ FoxP3+ Tregs among all CD4+ T-cells were determined in the spleens 2 days later. (K) Splenic tumor cells were sorted by fluorescence-activated cell sorting (FACS) from lymphoma-bearing mice and naïve splenic FoxP3/YFP+ Tregs from healthy mice were FACS-sorted and ex vivo co-cultured for 3 days. Activation and immunosuppressive Treg marker were examined by flow cytometry. (L) Sorted splenic tumor cells were cultured either alone or with naïve splenic Tregs isolated from healthy mice; tumor cell proliferation was measured by flow cytometry after 4 days of co-culture. Data in (H), (I) and (K) show individual experiments that are representative of at least two independently conducted studies; data in (J) and (L) are pooled from two experiments. Horizontal lines indicate medians throughout. Statistical comparisons were performed either by ordinary one-way analysis of variance or by unpaired t-test (Mann-Whitney). ns, not significant; *p<0.05, **p<0.01, ***p<0.005, ****p<0.001.

conversion into Foxp3/YFP$^+$ Tregs in tumor-bearing organs, which was not seen in non-tumor-bearing control mice (figure 1J). Furthermore, co-culturing of sorted, highly pure (>95%) tumor cells with naïve Tregs isolated from non-tumor-bearing animals' LNs for 3 days resulted in their increased expression of Ki67, CD44, CD27, Tbet, GITR, CD39 and other markers characteristic of tumor-infiltrating effector Tregs (figure 1K). Interestingly, co-culturing not only affected the immunophenotype of the Tregs, but also boosted the proliferation of the tumor cells, as assessed in a total of eight independent co-cultures (figure 1L). The combined data suggest that naïve T-cells differentiate into Foxp3$^+$ Tregs and acquire properties of effector Tregs in the lymphoma microenvironment, a process that appears to be tumor antigen-independent, locally driven and proportional to the tumor burden.

Single cell RNA-sequencing uncovers the transcriptional signature of lymphoma-infiltrating Tregs

To address how lymphoma-infiltrating Tregs differ from their normal LN counterparts using a complementary technique, we took advantage of Foxp3^{GFP} reporter mice to sort and single cell-sequence 20,000 Foxp3^{GFP}-positive Tregs per condition. Dimensionality reduction followed by Seurat clustering revealed nine Treg clusters that differed strongly in their relative abundance in tumor-bearing versus control LNs (figure 2A). Three clusters were exclusively present in lymphoma-bearing LNs, and the remaining six were vastly more abundant in the normal LNs (figure 2A). Hierarchical clustering of the top 80 most differentially expressed transcripts allowed the segregation of the nine populations (figure 2B) and confirmed several of the differentially regulated markers that were identified by flow cytometry, in addition to uncovering new ones. Several transcripts were highly intratumoral Treg-specific (among them the IL-7 receptor-encoded by *Il7r*), or at least predominantly expressed by tumor-infiltrating Tregs (*Tigit, Icos, Pdcd1*-encoding PD-1-, *Ifngr* and *Ctla4*) (figure 2B,C). Other transcripts (one example being *Stat1*) were exclusively expressed by control Treg clusters or were expressed by both control and tumor-infiltrating Treg clusters (*Bcl2, Stat4*; figure 2B,C). The combined data suggest substantial differences in Treg gene expression as a result of lymphoma infiltration, of which several could be confirmed also at the protein level (figure 2D). We further performed a TCR repertoire analysis on tumor-infiltrating versus control Tregs; this analysis uncovered hundreds of T-cell receptor α-chain (TRA) clusters in each sample of pooled Tregs from three to four mice per condition (309 TRA clusters in the control Tregs, 189 in the tumor Tregs; cut-off of >85% amino acid sequence similarity used for assignment to TRA cluster), which together accounted for ~2/3 of all Tregs. A total of 849 cells (control Tregs, vs 463 tumor Treg cells) were assigned to the most numerically dominant cluster; TRA-based Treg clusters did not segregate with the Treg clusters identified by scRNA sequencing of non-TCR transcripts, but rather mapped more or less

randomly to the Seurat clusters shown in figure 2A,E. The top 20 most abundant TRA clusters were found at similar frequencies among control and tumor-infiltrating Tregs (figure 2F). The combined data indicate that Tregs infiltrating MYC-driven lymphomas are not subject to clonal expansion, but show a very distinct (non-TCR) gene expression profile that clearly distinguishes them from normal LN Tregs.

Tregs infiltrate some but not all subtypes of human DLBCL

To assess whether the level of Treg infiltration observed in our model is reflective of Treg infiltration in human DLBCL cases, we stained 105 prospectively collected specimens from newly diagnosed patients with DLBCL in Switzerland (two independent cohorts, one unpublished and one published[36]) for FoxP3 and subjected their tumor DNA to amplicon sequencing of the 68 most recurrently mutated DLBCL genes. We found FoxP3-positive Tregs in close proximity to tumor cells, with some tumor cell/Treg pairs forming what appeared to be direct contacts (figure 3A). Roughly one half of cases exhibited evidence of substantial (>5%) FoxP3$^+$ Treg infiltration, whereas the other half contained negligible numbers of Tregs (figure 3B,C). GCB-DLBCL and ABC-DLBCL—distinguished using the Hans classification—were similarly likely to be infiltrated by Tregs (figure 3C). A comparison of the spectrum of mutations in DLBCL driver genes revealed that several mutations were over-represented in the Treg-infiltrated cases; among these were *SOCS1, ACTB* and *EZH2* (online supplemental figure S2A-C). Other mutations were over-represented in the Treg-negative cases; among these were *CD79B, KMT2D* and *DTX1* (online supplemental figure S2A-C). The parallel analysis of Treg infiltration of 206 DLBCL patient datasets publicly available through TCGA using cibersort[42] demonstrated that the 'MCD' genetic subtype (defined by co-occurring *MYD88* and *CD79* mutations) had the lowest Treg infiltration and *FOXP3* transcript levels, whereas the other three genetic subtypes introduced by Schmitz *et al* all had high Treg infiltration (figure 3D,E); over-represented mutations in the Treg-infiltrated cases included the *TNFRSF14* variant, whereas Treg$^{neg/low}$ cases were more likely to carry mutations in *MYD88, PIM1* and *CD79B* (figure 3F, online supplemental figure S2D). The combined data suggest that DLBCL exhibiting the characteristic 'MCD' subtype mutations are largely devoid of Treg infiltration; the Treg-infiltrated cases are less uniform in their mutational spectrum and include cases with canonical GCB-DLBCL mutations but also cases of the 'N1' genetic subtype.

Treg depletion reduces lymphoma growth and boosts anti-lymphoma effector T-cell responses

Given the high frequencies of effector Tregs within the lymphoma microenvironment in our experimental model, we set out to functionally assess the consequences of Treg depletion for lymphoma growth and anti-lymphoma immunity. Mice expressing the diphtheria toxin (DT) receptor specifically in the Treg compartment
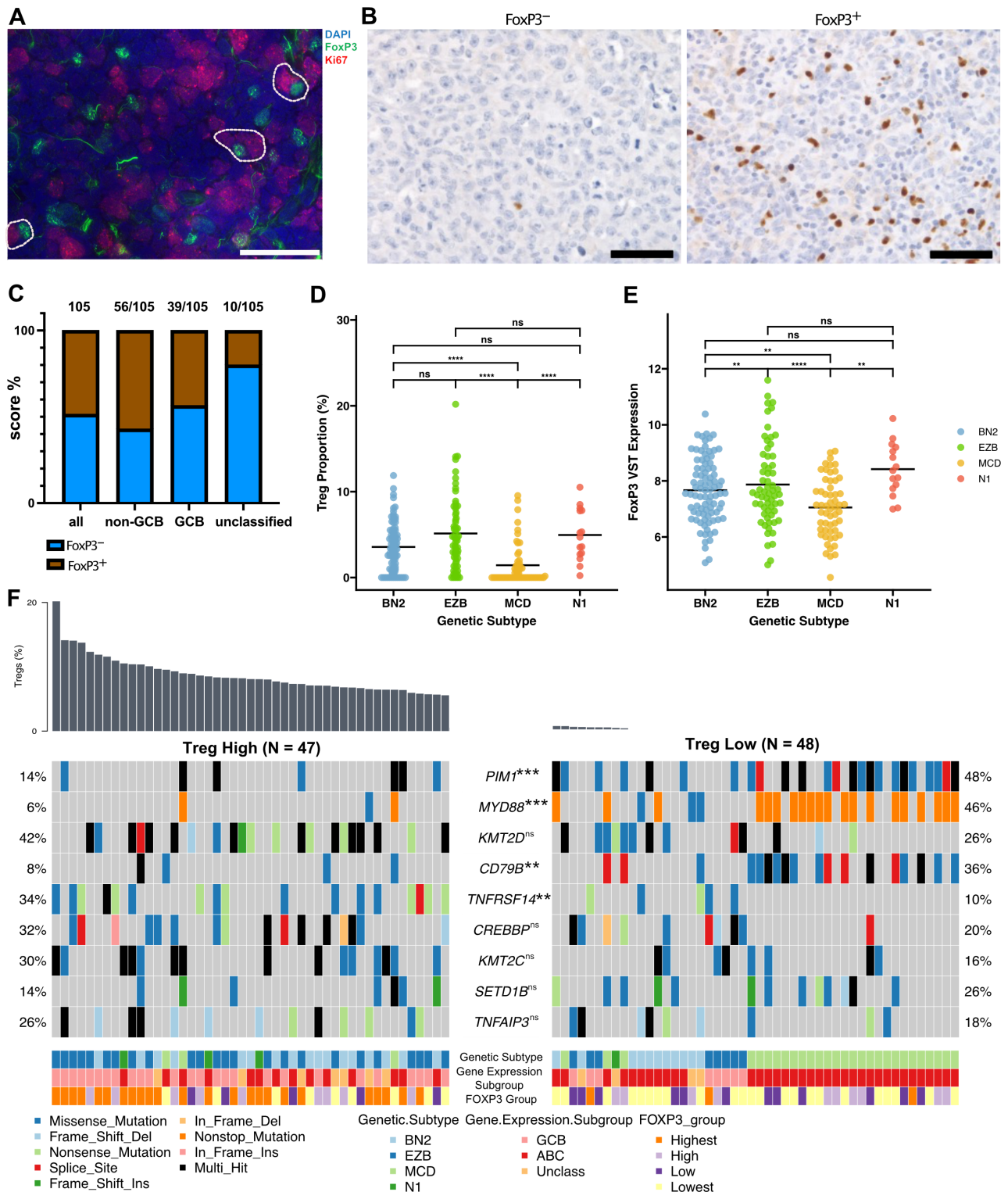
Figure 2 Lymphoma-infiltrating regulatory T-cells (Tregs) differ from normal lymph node (LN) Tregs with respect to their transcriptional signature. (A–C) Foxp3^YFP mice were intravenously injected with 1 Mio splenic MYC-overexpressing lymphoma cells. Foxp3/YFP+ Tregs from pooled axillary and inguinal LNs of three tumor-bearing and four non-tumor-bearing mice were sorted by fluorescence-activated cell sorting (FACS) at the study end point (day 11), labeled with antibody-conjugated hashtags and subjected to scRNA-Seq. UMAPs ("uniform manifold approximation and projection") (A) and heatmaps (B; 80 top differentially expressed genes) of the transcriptional profiles of 9 populations of tumor-infiltrating and control Tregs are shown alongside the expression of 10 representative transcripts in (C). (D) Single cell LN suspensions of tumor-bearing and control mice were subjected to flow cytometric analysis of the indicated surface markers; three differentially expressed surface markers are shown alongside a marker (ISOS) whose expression is unchanged. (E) TCR α-chain (TRA) sequences were extracted from the scRNAseq data and the top 10 most abundant clonotypes were mapped onto the Seurat clusters shown in (A). (F) Alluvial bar plots showing the proportions of the top 20 most abundant clonotypes among control and tumor-infiltrating Tregs. Statistical comparisons in (D) were performed by unpaired t-test (Mann-Whitney) and horizontal lines indicate medians throughout. ns, not significant; **p<0.01, ***p<0.005.

Figure 3 Regulatory T-cells (Tregs) infiltrate human diffuse large B-cell lymphoma (DLBCL) to variable extents. (A) Human fresh-frozen DLBCL cryosections were stained with anti-human FoxP3 and anti-human Ki67 antibodies. Nuclei were counterstained with 4′,6-diamidino-2-phenylindole (DAPI). White circles mark FoxP3+ Tregs in close contact with Ki67+ lymphoma cells. A representative section is shown of five independently stained sections. (B, C) Human DLBCL tissue microarrays (TMAs) comprising 105 cases were stained with anti-human FoxP3 antibody; FoxP3/Treg-negative and FoxP3/Treg-positive representative images are shown in (B) alongside the quantification of all cases in (C), also stratified by cell-of-origin (COO) status. Scale bar in (A) and (B), 50 µm. (D) Treg proportions (in %) infiltrating the four main DLBCL genetic subtypes were determined by performing cibersort on 206 DLBCL cases publicly available through TCGA and are shown stratified based on genetic subtype.[6] (E) FOXP3 transcript levels of the cases shown in (D). (F) Co-oncoplot of the top and bottom quartiles of Treg_high and Treg_low cases (assigned as described in D), showing the most common and differentially present mutations across the two groups. **p<0.01, ***p<0.005 indicate significantly or non-significantly (ns) differentially present mutations.

(Foxp3^DTR mice) received DT every 3 days starting on the day of lymphoma cell injection; this treatment led to a >90% reduction of Tregs in LNs, blood and other lymphoid and non-lymphoid tissues (online supplemental figure S3A and data not shown). Treg depletion resulted in a strongly reduced lymphoma burden in the LNs and spleen (figure 4A, online supplemental figure S3B); DT administration to wild-type mice had no effect (online supplemental figure S3C). The residual tumor cell population in Treg-depleted Foxp3^DTR mice failed to proliferate as determined by Ki67 staining (figure 4B). Continuous Treg depletion extended the lifespan of tumor-bearing mice by at least 3 days past the usual humane endpoint (day 11) of the experimental protocol, and measurably reduced the tumor burden as late as 14 days post injection (online supplemental figure S3D). The reduced lymphoma growth on Treg depletion was accompanied by strongly elevated frequencies of intratumoral CD4$^+$ and CD8$^+$ T-cells and by elevated interferon-γ (IFN-γ) production by both NK and CD4$^+$ T-cells, but not CD8$^+$ T-cells (online supplemental figure S3E-J). Spectral flow cytometry of the CD4$^+$ and CD8$^+$ T-cell compartments of Treg-replete and Treg-depleted tumor-bearing and control LNs further revealed large differences in these T-cell populations, with samples segregating into the three treatment groups (online supplemental figure S3K,L). Whereas CD4$^+$ and CD8$^+$ T-cells in control LNs were naïve (CD62L^{hi}, CD44^{neg}) and expressed the co-inhibitory receptor CTLA-4, their tumor-resident counterparts had downregulated CD62L and CTLA-4 but for the most part remained negative for CD44; only after Treg depletion, both compartments were fully activated and expanding as judged by their CD44, ICOS and Ki67 expression, and had differentiated into Tbet-positive type I cells; CD8$^+$ T-cells additionally upregulated the activation/exhaustion markers TIM3 and LAG3 (figure 4C–H, online supplemental figure S3M,N). To address whether the emergence of CD8$^+$, CD4$^+$ T-cells or NK cells is functionally relevant for the reduction of lymphoma growth associated with Treg depletion, all three populations were depleted by suitable antibodies alongside the depletion of Tregs by DT in Foxp3^DTR mice. Neither CD8$^+$ T-cell nor NK cell depletion reversed the effects of Treg depletion on lymphoma growth, despite a >90% reduction of the targeted populations; in contrast, the depletion of CD4$^+$ T-cells—in addition to Tregs—resulted in the restoration of lymphoma growth (figure 4I, online supplemental figure S3O-Q).

Various monoclonal antibodies that target the immunosuppressive activities of Tregs are currently in clinical development; among the most promising are antibodies blocking TIM3, TIGIT, CD73 and CD25 as well as a GITR agonistic antibody, especially when combined with immune checkpoint inhibitors such as anti-PD-L1.[43] To address whether any of the listed antibodies in clinical development would phenocopy the effects of DT-mediated Treg ablation, we administered each antibody, alone and/or in combination with anti-PD-L1 or anti-CTLA-4.

Neither the agonistic GITR-specific antibody, nor the TIGIT-blocking or CD25-blocking antibodies reduced the lymphoma burden relative to isotype control antibodies; in contrast, robust effects were obtained with anti-CD73 and anti-TIM3 blocking antibodies, alone and together with PD-L1 neutralization (figure 4J). The reduction of lymphoma growth was accompanied by a reduction of Treg infiltration under all effective treatments (figure 4K), with the latter being quite predictive of treatment success. Whether Treg depletion is a cause or consequence of the reduction in the lymphoma burden cannot be deduced from these data. The combined results suggest that Treg depletion effectively reduces the tumor burden, which can be attributed to reinvigorated CD4$^+$ effector T-cell, but not to CD8$^+$ T-cells or NK cell responses. Further experimental evidence suggests that Tregs suppress CD4$^+$ T-cells via their expression of the ATP hydrolyzing enzymes CD39 and CD73.

Tregs promote early stages of lymphoma engraftment and growth

To study the dynamics of lymphoma engraftment and growth, and of Treg support of these processes in more detail, we first tracked and quantified lymphoma cells and Tregs in the LNs and spleen, and also in the blood and bone marrow. Tumor cells were first detectable in blood, spleen and bone marrow at 6 days post injection, and appeared in the LNs 2 days later (figure 5A, online supplemental figure S4A). Treg frequencies among all CD4$^+$ T-cells differed substantially from one examined tissue to the other (being highest in the bone marrow at 50%, and lowest in the LNs and blood at <10%), and increased Treg frequencies were detected in all tissues on lymphoma cell injection (figure 5B, online supplemental figure S4B). The kinetics of increased Treg frequencies coincided with the kinetics of lymphoma cell appearance in the three tissues (day 8 in the LNs, day 6 in bone marrow and spleen), but not in blood, where only modest Treg increases were visible, and only with a 3-day delay at day 9 (figure 5A,B, online supplemental figure S4A,B). To address at which point in time Treg depletion would have the strongest impact on the lymphoma burden, we initiated DT treatments either 2 days before, or on days 1, 2, 3, 4 or 5, or on day 9 post tumor cell injection, and continued the treatment until the study endpoint. Only the early depletion of Tregs—initiated up until day 3, but not later depletion effectively reduced the lymphoma burden, and lymphoma cell proliferation as assessed by Ki67 staining (figure 5C,D). Early, but not late Treg depletion further also boosted the intratumoral CD4$^+$ and CD8$^+$ effector T-cell responses that coincided with tumor control (online supplemental figure S4C-E). Indeed, a few doses of DT administered up until day 4 (resulting in the restoration of Tregs back to normal levels by the end of the study) were as effective as continuous Treg depletion until the study endpoint at suppressing the lymphoma burden (figure 5E–G). This was accompanied by increased CD4$^+$ T-cell activation, as indicated by
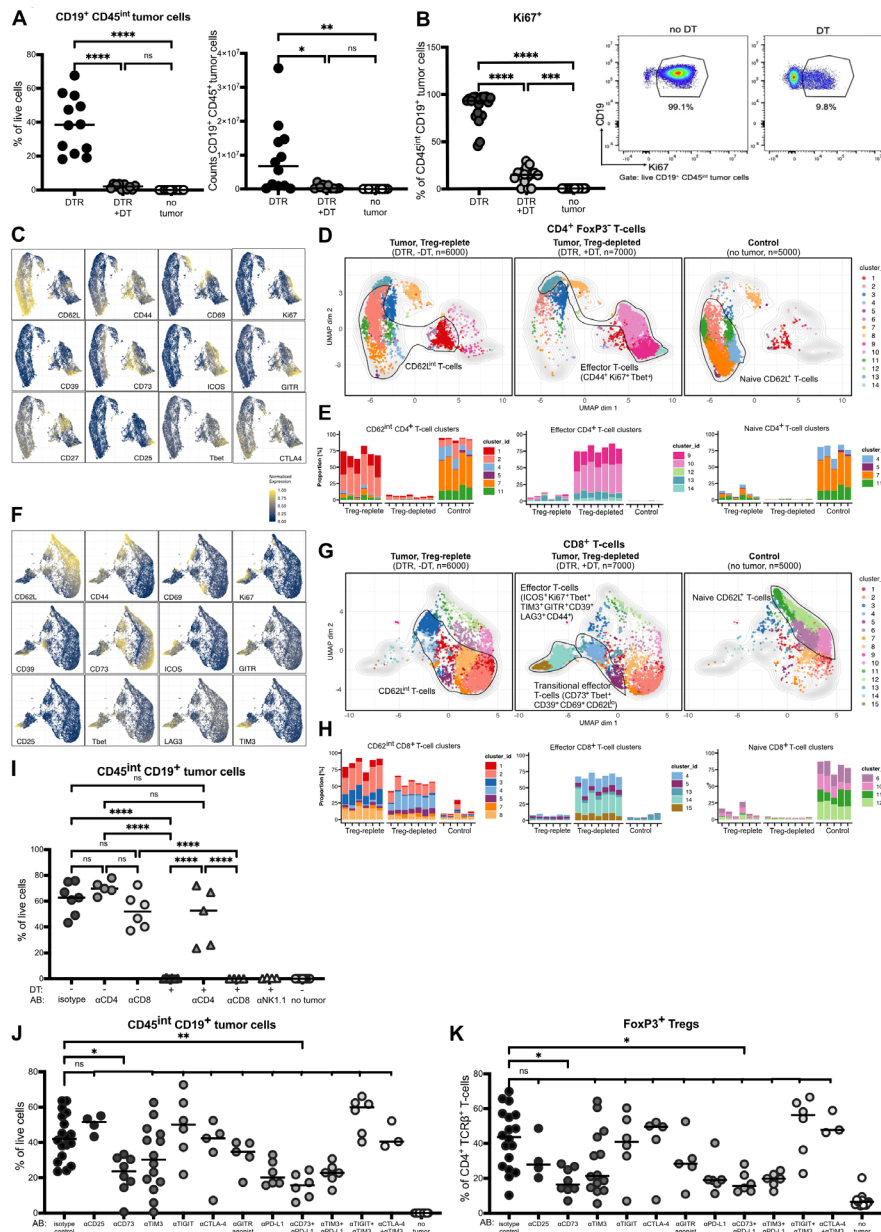
Figure 4 Lymphoma-infiltrating regulatory T-cells (Tregs) suppress CD4^{+}, but not CD8^{+} T-cell or natural killer (NK) cell responses to support lymphoma growth. (A–H) FoxP3[DTR/GFP] mice ('DTR') were intravenously injected with 1 Mio splenic MYC-overexpressing lymphoma cells and intraperitoneally injected or not, starting on the same day and continued every 3 days thereafter, with 20 ng/g body weight diphtheria toxin (+DT). Mice were examined at the study endpoint (11 days post injection) for their lymphoma burden in lymph nodes (LNs) (frequencies and absolute numbers (A)), their LN frequencies of Ki67^{+} proliferating tumor cells (summary plot and representative plots (B)) and the immunophenotypes of their LN CD4^{+} (C–E) and CD8^{+} (F–H) T-cell compartments, relative to non-tumor-bearing controls (no tumor). Marker UMAPs ("uniform manifold approximation and projection") are shown in (C) and (F); condition UMAPs are shown for 14 CD4^{+} T-cell and for 15 CD8^{+} T-cell populations in (D) and (G), alongside the quantification of the most differentially present clusters in all examined mice (n=5–7) in (E) and (H). Naïve, CD62L^{int} transitional and effector populations are marked in (D) and (G). Data in (A) and (B) are pooled from three experiments; data in (C)–(H) are from one experiment, but representative of three. (I) Mice were transplanted with tumor cells as described in (A)–(H), and intraperitoneally injected with an initial dose of 300 µg of anti-mouse CD4, CD8 and NK1.1 neutralizing antibody or isotype control antibody followed by twice weekly injections of 200 µg intraperitoneal either alone or together with 20 ng/g diphtheria toxin intraperitoneal. Mice were sacrificed on day 11 and the tumor burden in axillary and inguinal lymph node preparations was assessed. (J, K) C57BL/6 mice were transplanted with lymphoma cells as described in (A)–(H), and intraperitoneally injected, starting on the same day, with an initial dose of 300 µg of anti-mouse (α)CD25, αCD73, αTIM3, αTIGIT (100 µg/dose), αGITR agonist, αPD-L1 and αCTLA4 neutralizing antibody, isotype control antibody or the indicated combination of antibodies, which was followed by 200 µg maintenance doses twice a week. Tumor burden (J) and Treg frequencies (K) were determined by flow cytometry. Results in (I)–(K) are pooled from two to three experiments per experimental group. Statistical comparisons were performed by ordinary one-way analysis of variance. ns, not significant; *p<0.05, **p<0.01, ***p<0.005, ****p<0.001. Horizontal lines indicate medians.
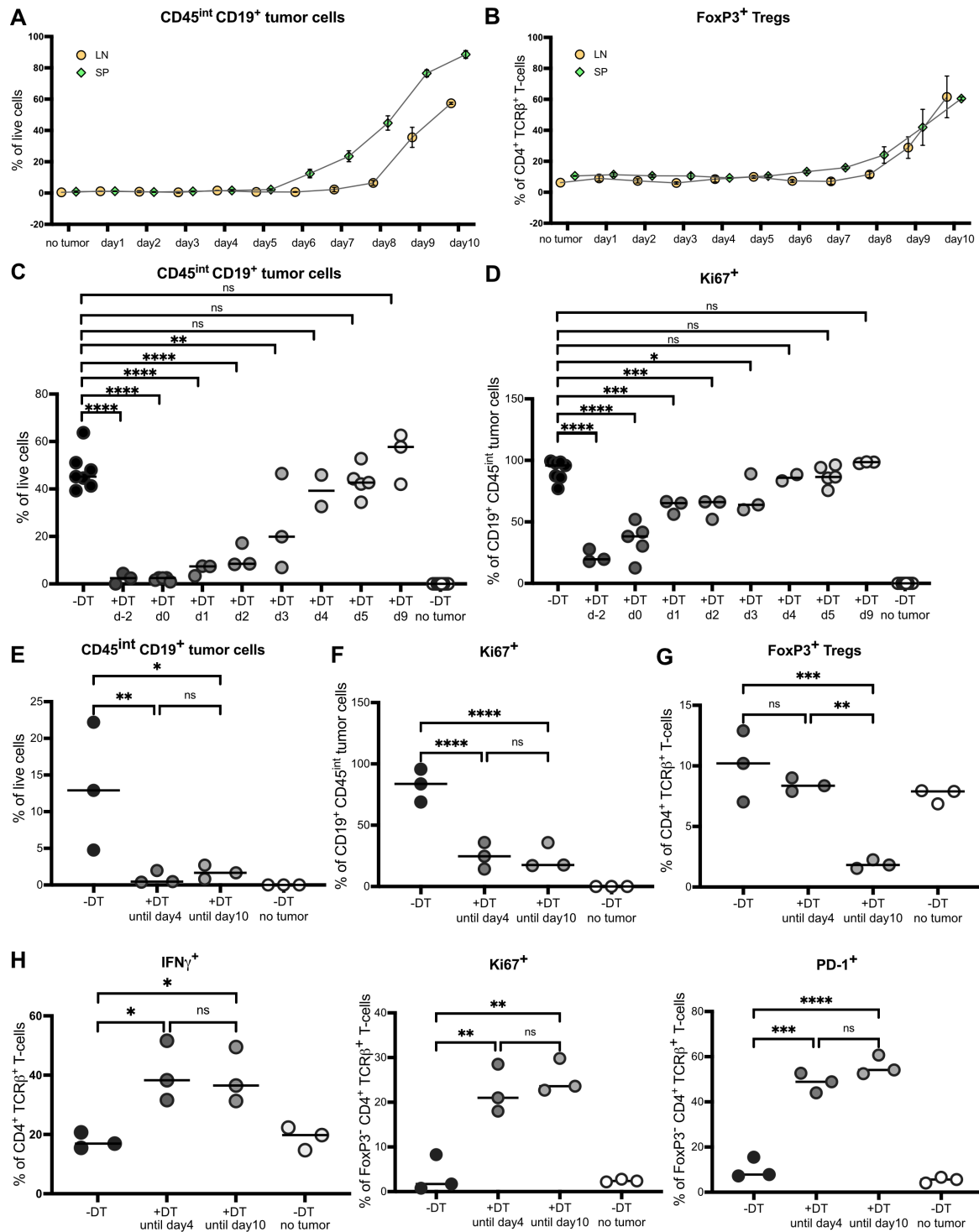
Figure 5 Regulatory T-cells (Tregs) act during early stages of lymphomagenesis. (A, B) C57BL/6 mice were intravenously injected with 1 Mio splenic MYC-overexpressing lymphoma cells and examined with respect to the lymph node (LN) lymphoma burden (A) and intratumoral Treg frequencies (B) at the indicated time points post transplantation. Means±SD are shown for three mice per group. (C, D) FoxP3$^{DTR/GFP}$ mice were intravenously injected with 1 Mio splenic MYC-overexpressing lymphoma cells and 20 ng/g diphtheria toxin was administered intraperitoneal starting either 2 days prior to tumor cell inoculation, on the day of inoculation, or at 2, 3, 4, 5 and 9 days post inoculation; treatments were continued until the study endpoint (11 days post injection) with injections every 3 days. Tumor burden (C) and frequencies of Ki67$^+$ proliferating tumor cells (D) were determined by flow cytometry. (E–H) FoxP3$^{DTR/GFP}$ mice were intravenously injected with 1 Mio splenic MYC-overexpressing lymphoma cells; 20 ng/g diphtheria toxin was injected intraperitoneal on the day of tumor cell inoculation followed by a second and final injection on day 4, or on days 4, 7 and 10. Tumor burden (E), frequencies of Ki67$^+$ proliferating tumor cells (F), Treg frequencies (G) and frequencies of IFNγ$^+$, Ki67$^+$ and PD-1$^+$ CD4$^+$ T-cells (H) were determined by flow cytometry. Horizontal lines indicate medians. Statistical comparisons were performed by ordinary one-way analysis of variance. ns, not significant; *p<0.05, **p<0.01, ***p<0.005, ****p<0.001.

elevated levels of IFN-γ, Ki67 and PD-1 (figure 5H). The combined results indicate that Tregs facilitate lymphoma cell engraftment and growth in our experimental model, likely by affecting CD4$^+$ effector T-cell priming, and have a critical role long before elevated Treg levels (and lymphoma cells) appear in affected tissues and the bloodstream.

Treg-specific IL-2 starvation reduces Treg infiltration and lymphoma growth

As IL-2 is a key cytokine driving Treg differentiation by promoting Foxp3 expression in naïve T-cells,[44] we asked whether Treg-specific IL-2 starvation might phenocopy the effects of Treg ablation in Foxp3^{DTR} mice, and whether tumor B-cells might directly act as a source of IL-2. Indeed, we found that MYC-expressing lymphoma cells produce large amounts of IL-2, which is not the case for normal B-cells in the same LNs (figure 6A). Human DLBCL cell lines vary in their IL-2 expression, with some expressing enormous amounts, others modest amounts and yet others no IL-2 whatsoever (online supplemental figure S5A). To specifically starve Tregs, but not effector T-cells of IL-2, we took advantage of an antibody that selectively prevents IL-2 binding by the α-chain of the IL-2 receptor, CD25, which is expressed by Tregs at much higher levels than by effector T-cells.[30] Anti-IL-2 antibody treatment reduced Treg frequencies without affecting CD4$^+$ or CD8$^+$ effector T-cell frequencies, and dose-dependently reduced the lymphoma burden (figure 6B and C, online supplemental figure S5B); CD25 expression was indeed much higher on tumor-infiltrating Tregs than on intratumoral CD4$^+$ and CD8$^+$ T-cells (online supplemental figure S5C). The small residual Treg population that escaped starvation did not immunophenotypically differ from tumor-infiltrating Tregs in isotype-treated tumor-bearing mice as determined by spectral flow cytometry (figure 6D, online supplemental figure S5D). Anti-IL-2 treatment had no effect on the tumor burden in T-cell (and Treg)-deficient RAGγc$^{-/-}$ mice (figure 6E), suggesting that the beneficial effects of IL-2 neutralization are probably not tumor cell-intrinsic. Interestingly, IL-2 neutralization had no effect on the quantity or immunophenotype of normal Tregs in control mice, the surface marker expression and frequencies of which were unchanged; indeed, Tregs in non-tumor-bearing LNs expressed much less CD25 than their tumor-infiltrating counterparts (figure 6F,G, online supplemental figure S5E,F). The combined results provide experimental evidence for the efficacy of Treg-specific IL-2 starvation in controlling lymphoma growth in this MYC-driven model.

IL-2 neutralization synergizes with CD40 activation in promoting durable responses

As Treg starvation alone is unlikely to confer long-term survival benefits in our aggressive lymphoma model, we asked whether anti-IL-2 therapy would synergize with other immunotherapies in promoting durable responses beyond the usual 10-day timeframe of our model. As we

found aberrantly low expression of the co-stimulatory surface marker CD40 on tumor B-cells relative to normal B-cells (figure 7A), and detected a strong increase in CD40 expression on tumor B-cells but not normal B-cells on Treg depletion (figure 7B), we set out to determine whether targeting CD40 using an agonistic antibody would reduce the lymphoma burden, with and without additional Treg depletion by IL-2 neutralization. Twice-weekly injection of a CD40-specific agonistic antibody effectively reduced the lymphoma burden and lymphoma cell proliferation (figure 7C,D). In fact, a single anti-CD40 injection administered on the day of tumor cell injection was sufficient to prevent lymphoma growth until the humane endpoint was reached for all isotype antibody-treated mice (figure 7C,D). As CD40 activation led to a strong Fas upregulation on MYC-expressing lymphoma cells (online supplemental figure S6A), and simultaneously to Fas ligand (FasL) upregulation on NK cells (online supplemental figure S6B), we asked whether the tumoricidal activity of the CD40 agonistic antibody required the cytotoxic activities of T-cells or NK cells, or of FasL. CD40 activation was as effective in RAG2γc$^{-/-}$ mice-lacking T-lymphocytes and B-lymphocytes and NK cells—as in wild-type C57BL/6 mice at reducing lymphoma growth (figure 7E) and could not be counteracted by FasL blockade (online supplemental figure S6C). A single dose of CD40 agonist administered 1 day prior to the study endpoint was sufficient to reduce the lymphoma burden (figure 7E) and allowed us to determine that tumor cells became annexin-V-positive under treatment, indicating apoptotic cell death induced by CD40 activation (figure 7F). Normal B-cells in the same lymph nodes did not undergo increased apoptosis on CD40 activation, and even appeared to proliferate more (online supplemental figure S6D,E).

To address how common CD40 expression is among patients with DLBCL, we stained 110 samples from the two prospectively collected patient cohorts mentioned earlier for CD40. CD40 expression varied radically across patients, with some tumors expressing no CD40 whatsoever and others expressing copious amounts (figure 7G). Roughly one-fourth of cases expressed high, moderate, low levels of, or no CD40, respectively (figure 7H). No bias towards ABC-DLBCL or GCB-DLBCL subtype was observed (figure 7H). A similar variability of CD40 expression was observed in a panel of DLBCL cell lines (online supplemental figure S6F). Treg infiltration and CD40 expression appeared to be independent variables in the 94 patients with DLBCL for whom both CD40 and FoxP3 immunohistochemical stainings were evaluable (figure 7I).

Although highly efficient in the short term at reducing the lymphoma burden, CD40 activation alone did not sustain durable responses, neither if the treatment was continued for another 2 weeks, nor if it was discontinued at the usual study endpoint of 10 days (figure 7J,K). However, when CD40 activation was combined with IL-2 neutralization, with both treatments beginning on the
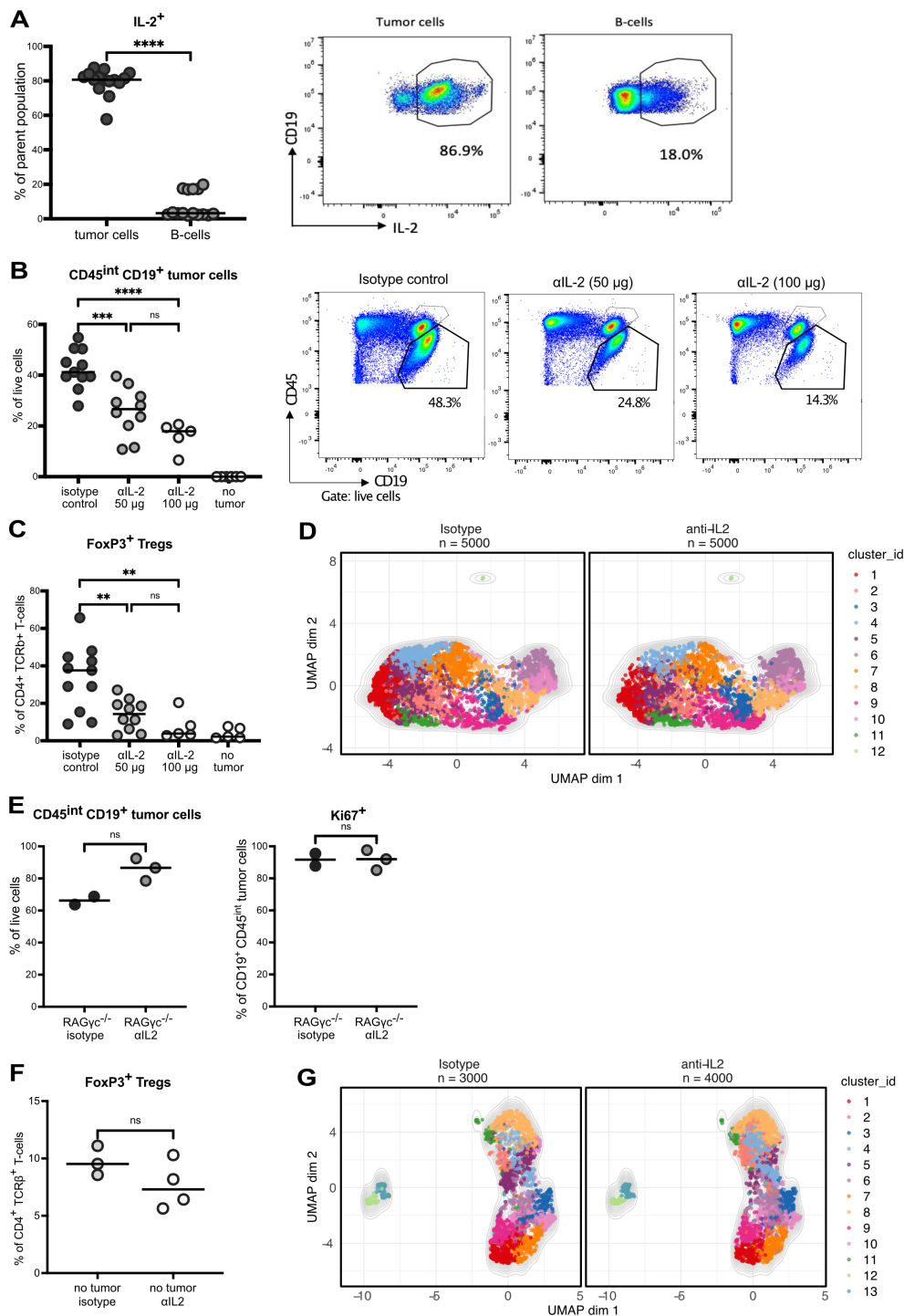
Figure 6 Anti-IL-2 treatment reduces regulatory T-cell (Treg) infiltration and lymphoma growth. (A) C57BL/6 mice were injected intravenously with 1 Mio splenic MYC-overexpressing lymphoma cells. Interleukin-2 (IL-2) expression by tumor cells and normal B-cells in single cell lymph node (LN) preparations was determined by intracellular cytokine staining (summary plot and representative flow cytometry plots are shown in (A) at the study endpoint. (B–D) Mice were treated Intraperitoneally twice weekly with either 50 µg or 100 µg anti-IL-2 antibody or isotype control antibody starting on the day of tumor cell inoculation. Tumor burden (summary plot and representative plots, (B) and Treg frequencies (C) were determined by flow cytometry. Condition UMAPs ("uniform manifold approximation and projection") of Tregs from anti-IL-2 (100 µg) or isotype control antibody-treated mice are shown in (D). (E) RAGγc$^{-/-}$ mice were injected with lymphoma cells and treated with 100 µg of anti-IL-2 antibody or isotype control antibody as described in (B)–(D). Frequencies of tumor cells, and Ki67$^+$ tumor cells were determined at the study endpoint (day 10). (F, G) Non-tumor-bearing C57BL/6 mice were treated as described in (E) and examined on day 10 with respect to their LN Treg frequencies (F) and Treg immunophenotypes as determined by spectral flow cytometry (G). Data in (A) and (B) are pooled from three studies; data in (E) and (F) are from one study. Statistical comparisons were performed either by ordinary one-way analysis of variance or by unpaired t-test (Mann-Whitney). ns, not significant; **p<0.01, ***p<0.005, ****p<0.001. Horizontal lines indicate medians.
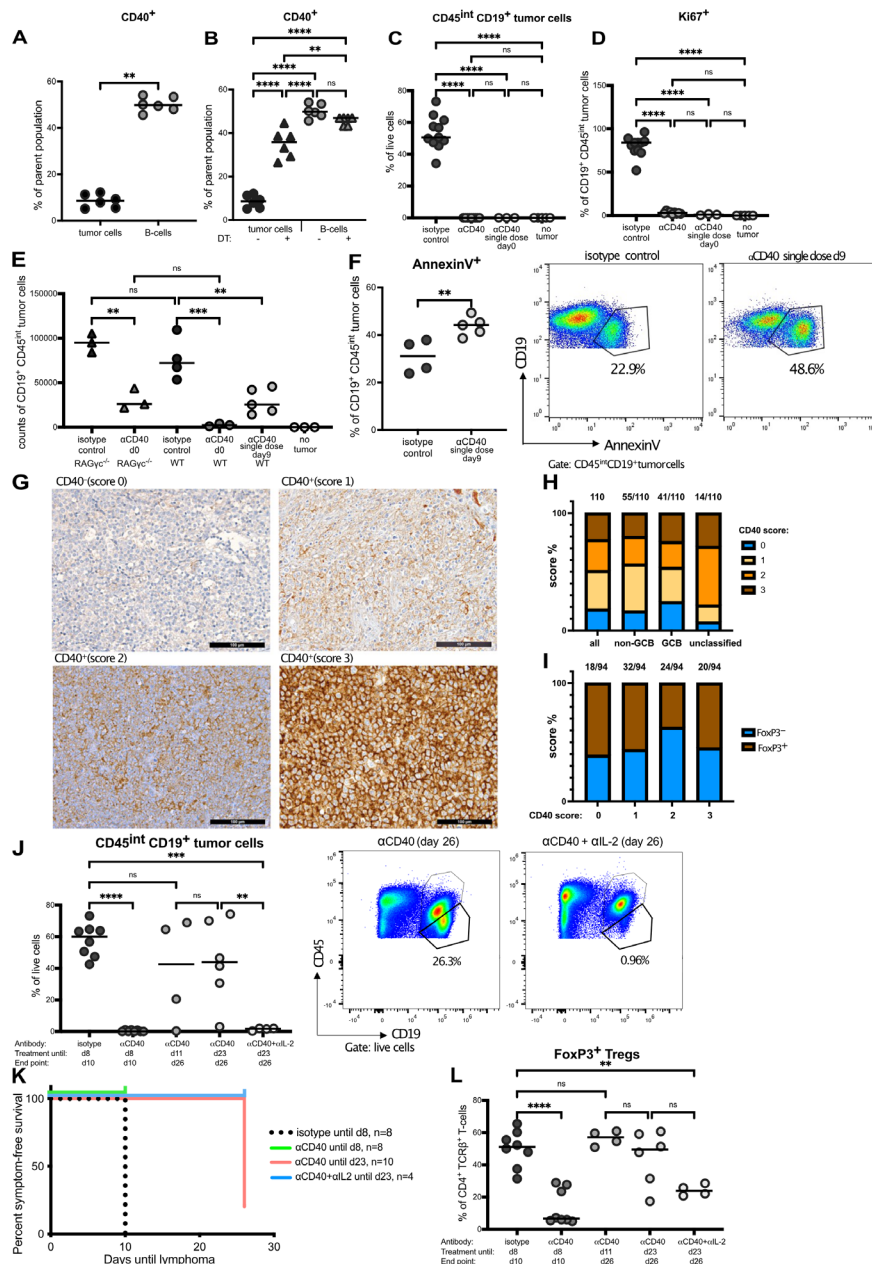
Figure 7 Regulatory T-cell (Treg) depletion and CD40-driven cytotoxicity synergize for sustained durable responses. (A) C57BL/6 mice were injected intravenously with 1 Mio splenic MYC-overexpressing lymphoma cells. CD40 surface expression of tumor cells and normal B-cells in single cell lymph node (LN) preparations was determined by flow cytometry. (B) FoxP3$^{DTR/GFP}$ mice were injected with lymphoma cells; 20 ng/g diphtheria toxin was injected intraperitoneally every 3 days. CD40 expression on tumor cells and normal B-cells was evaluated by flow cytometry on day 10 post transplantation. (C, D) C57BL/6 mice were treated with either a single 100 µg dose of anti-CD40 agonistic antibody or by twice weekly injections of anti-CD40 or isotype control antibody. Frequencies of lymphoma cells (C) and Ki67$^+$ lymphoma cells (D) were determined by flow cytometry. (E) RAGγc$^{-/-}$ or C57BL/6 mice were injected with lymphoma cells and treated with 100 µg anti-CD40 agonistic antibody or isotype control antibody either at from the day of tumor cell inoculation or only on day 9 (1 day prior to the study endpoint). Absolute numbers of tumor cells are shown in (E). (F) AnnexinV$^+$ apoptotic lymphoma cells were quantified by flow cytometry on single dose (day 9) αCD40 or isotype control antibody treatment; a summary plot and representative plots are shown. (G–I) Human FFPE DLBCL specimens spotted on tissue microarrays (TMAs) were stained for CD40; representative images are shown for each score (0–3; G) and the scores for all 110 analyzed cases are shown in (H).The frequencies of FoxP3+ and FoxP3– cases are shown in (I) for each CD40 score. (J–L) C57BL/6 mice were injected with lymphoma cells and treated either with anti-CD40 agonistic antibody, isotype control antibody or with a combination of anti-CD40 and anti-IL-2 antibody (100 µg/dose) for the indicated durations. Mice were sacrificed on either day 10 or on day 26, and the tumor burden (summary plot and representative plots; J) was determined by flow cytometry. Kaplan-Meier curves and Treg frequencies are shown in (L). Data in (B), (C), (D), (J) and (K) are pooled from two studies, all others are from one representative study of two. Statistical comparisons were performed either by ordinary one-way analysis of variance or by unpaired t-test (Mann-Whitney). ns, not significant; **p<0.01, ***p<0.005, ****p<0.001. Horizontal lines indicate medians.

day of tumor cell injection, all mice on the dual treatment were symptom-free and had a minimal or undetectable tumor burden at the study endpoint (figure 7J,K). Treg infiltration was reflective of the tumor burden, and lowest in the absence of tumor and under IL-2 neutralization (figure 7L). The combined results implicate CD40 as a promising target enabling direct killing by apoptosis of a subset of CD40-expressing DLBCL; the response to CD40-directed therapy is further improved by Treg depletion.

DISCUSSION

We show here that (1) Tregs are abundant, highly immunosuppressive cells in the lymphoma microenvironment in our experimental model of MYC-driven B-cell lymphoma, and in several genetic subtypes of DLBCL, that (2) Tregs are induced in the lymphoma microenvironment and sustained by tumor-derived IL-2 and that (3) their DT-driven or antibody-driven ablation strongly reduces the lymphoma burden, especially when combined with a direct cytotoxic immunotherapy such as CD40 stimulation. Several of the functional and immunosuppressive effector Treg markers identified here in the lymphoma context by spectral flow cytometry and scRNA-seq have previously been assigned to Tregs infiltrating the tumor microenvironment of solid organ malignancies, and are well known to maintain Treg functional stability and/or to enhance intratumoral Treg suppressive activities.[45] Examples include Nrp-1, which marks Tregs associated with poor prognosis in human melanoma and head and neck squamous cell carcinoma; its loss specifically in Tregs leads to control of B16 melanoma.[46 47] TIGIT and CTLA-4 are examples of inhibitory receptors that are not only overexpressed on tumor-infiltrating relative to naïve Tregs in tumor-bearing mice and patients, but also contribute functionally to Treg suppressive activity and may be targeted to boost tumor rejection,[29 45 48] although not in our hands when using a TIGIT-blocking antibody. The effector Tregs in our experimental model appear to arise via an intermediate state that is characterized by loss of CD62L but lacks expression of CD44 or any of the immunosuppressive markers listed above; our adoptive transfer experiments suggest that Tregs are converted locally in the lymphoma microenvironment from CD4$^+$ precursors, rather than being recruited as fully functional, mature cells.

Tregs were previously shown[22 26] and confirmed again here to infiltrate DLBCL at considerable densities. Cibersort analysis of TCGA data and our own in situ observations indicated that the MCD genetic subtype was less infiltrated than other genetic subtypes[6]; indeed, signature mutations such as the $MYD88^{L265P}$, $PIM1$ and activating $CD79B$ mutations were significantly overrepresented in the Treg-negative cases. This observation could be confirmed for $CD79B$ in our independent Swiss cohorts, whereas the stratification by cell-of-origin (COO) was not helpful in predicting Treg infiltration, as the two genetic ABC-DLBCL subtypes (N1, MCD) have strongly divergent

Treg infiltration that masks potential differences between the GCB-DLBCL and ABC-DLBCL COO subtypes.

The presence of effector Tregs, characterized by co-expression of CTLA-4 or TIM-3 with Foxp3, in the only two studies to date taking markers other than Foxp3 into account[24 26] was of strong negative prognostic importance. Indeed, ablation of Tregs, either in a genetic, DT-driven model or by selective Treg starvation of their growth factor IL-2, substantially and consistently reduced the tumor burden in all examined organs in our MYC-driven model. The tumor-promoting effect of Tregs could be attributed to their effects on CD4$^+$, but not CD8$^+$ T-cells or NK cells. Interestingly, our own earlier immunohistochemical analysis comparing Treg infiltration of DLBCL arising in immunocompetent versus immunodeficient patients provides circumstantial evidence for an exclusive role of Tregs in the immunocompetent patient, as we found Tregs to be almost completely absent in post-organ transplant DLBCL patients on immunosuppressive therapy.[28]

IL-2 acts at various stages of Treg differentiation, driving Foxp3 expression during Treg development, and promoting the long-term survival and suppressive activity of mature Tregs.[44] Selectively interfering with IL-2 signaling in Tregs (but not other IL-2-consuming T-cells) by preventing IL-2 binding to the main ligand-binding subunit of IL-2R in Tregs, CD25, phenocopied the effects of DT-driven Treg depletion. The human variant of the antibody we used here is in clinical development as an IL-2/anti-IL-2 antibody complex fusion (not to be confused with the naked antibody administered in our study), which directs IL-2 to CD8$^+$ T-cells resulting in their efficient expansion and in tumor immune control in various solid cancer models.[30 49] The crystal structure of the human version of the antibody has revealed that it occupies the CD25-binding epitope of IL-2 and precisely overlaps with CD25, which explains why it prevents binding of IL-2 to the trimeric IL-2R on Tregs (consisting of CD25, CD122 and the common gamma chain γc) in our hands, while—in complex with IL-2—selectively targeting the dimeric IL-2R (consisting of CD122 and γc) on CD8$^+$ T-cells.[30] As anti-IL-2 treatment efficiently depleted tumor-infiltrating CD25^{hi} effector Tregs in our study, but left the naïve Treg compartment in control mice largely intact and immunophenotypically unaltered, it represents an attractive alternative to other Treg-targeting therapeutic strategies that are potentially less tumor-Treg-specific.[43] High level IL-2 production is a fairly common adaptation in DLBCL as 4 of the 13 examined cell lines secreted copious amounts of the cytokine when in culture.

IL-2 starvation and Treg depletion by DT were effective in short-term studies, but—at least as monotherapy—failed to extend the survival of our tumor-bearing mice by more than a few days. As CD40 expression by lymphoma B-cells was aberrantly low relative to normal B-cells, but could be restored by Treg depletion, we investigated whether activation of CD40 by an agonistic antibody might synergize with Treg depletion in eradicating tumors and

generating durable responses. This was indeed the case as mice on anti-IL-2/anti-CD40 combination treatment survived for 2 weeks past the usual humane endpoint, with only minimal evidence of residual tumor cells at the study endpoint.

CD40-directed agonistic antibodies were not initially developed to directly target, and kill, CD40-expressing tumor cells but rather to increase the number and quality of tumor-infiltrating T-cells and thereby, response effectiveness, in CD40-negative solid organ malignancies.[50–52] In such settings of CD40-negative malignancies, CD40 on antigen-presenting cells (APCs) plays a central role in stimulating immune synapses, including during T-cell priming, when its interaction with the CD40 ligand (CD40L) licenses DCs to activate antigen-specific T-cells.[53] The situation is complicated in B-cell malignancies by varying extents of tumor-intrinsic CD40 expression; chronic lymphocytic leukaemia, Burkitt lymphoma and DLBCL cells have all been reported to express CD40 and to respond to CD40 activation with activation-induced cell death (AICD) in vitro and/or in experimental models.[54–56] Interestingly, normal and neoplastic B-cells respond differently to CD40 agonistic antibodies and soluble CD40L, whereas CD40 stimulation promotes differentiation and growth of normal B-cells in vitro (confirmed here also in vivo), malignant B-cells typically undergo AICD when exposed to CD40 agonistic antibodies or soluble CD40L,[56 57] or are sensitized to other cell death-inducing agents.[54] An active CD40 signaling pathway was found to be predictive of treatment response in a phase I trial of dacetuzumab, a CD40-specific antibody with partial agonistic activity[56] and CD40 expression has generally emerged as a favorable prognostic marker in patients on CHOP or R-CHOP.[58–60] Our experimental data do not completely rule out tumor-cell extrinsic effects of CD40 targeting, but the comparable levels of tumor reduction in WT and RAGγc$^{-/-}$ mice suggest that direct killing by CD40 activation is the dominant mechanism of tumor control in our model.

Our combined data from both experimental mouse studies and patient data provide a strong rationale for targeting Tregs in highly Treg-infiltrated DLBCL, especially in combination with cytotoxic immunotherapy directed at CD40.

ORCID iDs
Kristin Stirm http://orcid.org/0000-0002-8870-164X
Dominique Stark http://orcid.org/0000-0002-3214-7950
Anne Müller http://orcid.org/0000-0002-1368-8276

REFERENCES

1 Coiffier B, Thieblemont C, Van Den Neste E, *et al*. Long-Term outcome of patients in the LNH-98.5 trial, the first randomized study comparing rituximab-CHOP to standard CHOP chemotherapy in DLBCL patients: a study by the Groupe d'etudes des Lymphomes de l'Adulte. *Blood* 2010;116:2040–5.

2 Coiffier B, Lepage E, Briere J, *et al*. Chop chemotherapy plus rituximab compared with CHOP alone in elderly patients with diffuse large-B-cell lymphoma. *N Engl J Med* 2002;346:235–42.

3 Chow VA, Shadman M, Gopal AK. Translating anti-CD19 CAR T-cell therapy into clinical practice for relapsed/refractory diffuse large B-cell lymphoma. *Blood* 2018;132:777–81.

4 Basso K, Dalla-Favera R. Germinal centres and B cell lymphomagenesis. *Nat Rev Immunol* 2015;15:172–84.

5 Chapuy B, Stewart C, Dunford AJ, *et al*. Molecular subtypes of diffuse large B cell lymphoma are associated with distinct pathogenic mechanisms and outcomes. *Nat Med* 2018;24:679–90.

6 Schmitz R, Wright GW, Huang DW, *et al*. Genetics and pathogenesis of diffuse large B-cell lymphoma. *N Engl J Med* 2018;378:1396–407.

7 Menter T, Juskevicius D, Alikian M, *et al*. Mutational landscape of B-cell post-transplant lymphoproliferative disorders. *Br J Haematol* 2017;178:48–56.

8 Challa-Malladi M, Lieu YK, Califano O, *et al*. Combined genetic inactivation of beta2-microglobulin and CD58 reveals frequent escape from immune recognition in diffuse large B cell lymphoma. *Cancer Cell* 2011;20:728–40.

9 Pasqualucci L, Dominguez-Sola D, Chiarenza A, *et al*. Inactivating mutations of acetyltransferase genes in B-cell lymphoma. *Nature* 2011;471:189–95.

10 Hashwah H, Schmid CA, Kasser S, *et al*. Inactivation of CREBBP expands the germinal center B cell compartment, down-regulates MHCII expression and promotes DLBCL growth. *Proc Natl Acad Sci USA* 2017;114:9701–6.

11 Jiang Y, Ortega-Molina A, Geng H, *et al*. CREBBP inactivation promotes the development of HDAC3-dependent lymphomas. *Cancer Discov* 2017;7:38–53.

12 Zhang J, Vlasevska S, Wells VA, *et al*. The crebbp acetyltransferase is a haploinsufficient tumor suppressor in B-cell lymphoma. *Cancer Discov* 2017;7:322–37.

13 Georgiou K, Chen L, Berglund M, *et al*. Genetic basis of PD-L1 overexpression in diffuse large B-cell lymphomas. *Blood* 2016;127:3026–34.

14 Kataoka K, Shiraishi Y, Takeda Y, *et al*. Aberrant PD-L1 expression through 3'-UTR disruption in multiple cancers. *Nature* 2016;534:402–6.

15 Wang C, Shi F, Liu Y, *et al*. Anti-Pd-1 antibodies as a salvage therapy for patients with diffuse large B cell lymphoma who progressed/relapsed after CART19/20 therapy. *J Hematol Oncol* 2021;14:106.

16 Smith SD, Till BG, Shadman MS, *et al*. Pembrolizumab with R-CHOP in previously untreated diffuse large B-cell lymphoma: potential for biomarker driven therapy. *Br J Haematol* 2020;189:1119–26.

17 Ansell SM. The highs and lows of immune-checkpoint blockade in lymphoma. *Cancer Immunol Res* 2019;7:696–700.

18 Ansell SM, Minnema MC, Johnson P, *et al*. Nivolumab for relapsed/refractory diffuse large B-cell lymphoma in patients ineligible for or having failed autologous transplantation: A single-arm, phase II study. *J Clin Oncol* 2019;37:481–9.

19 Xu-Monette ZY, Xiao M, Au Q, *et al*. Immune profiling and quantitative analysis decipher the clinical role of immune-checkpoint expression in the tumor immune microenvironment of DLBCL. *Cancer Immunol Res* 2019;7:644–57.

20 Autio M, Leivonen SK, Bruck O, *et al*. Immune cell constitution in the tumor microenvironment predicts the outcome in diffuse large B-cell lymphoma. *Haematologica* 2021;106:718–29.

21 Keane C, Vari F, Hertzberg M, *et al*. Ratios of T-cell immune effectors and checkpoint molecules as prognostic biomarkers in diffuse large B-cell lymphoma: a population-based study. *Lancet Haematol* 2015;2:e445–55.

22 Tzankov A, Meier C, Hirschmann P, *et al*. Correlation of high numbers of intratumoral Foxp3+ regulatory T cells with improved survival in germinal center-like diffuse large B-cell lymphoma, follicular lymphoma and classical Hodgkin's lymphoma. *Haematologica* 2008;93:193–200.

23 Chang C, Chen Y-P, Medeiros LJ, *et al*. Higher infiltration of intratumoral CD25+ Foxp3+ lymphocytes correlates with a favorable prognosis in patients with diffuse large B-cell lymphoma. *Leuk Lymphoma* 2021;62:76–85.

24 Zhong W, Liu X, Zhu Z, *et al*. High levels of tim-3+foxp3+treg cells in the tumor microenvironment is a prognostic indicator of poor survival of diffuse large B cell lymphoma patients. *Int Immunopharmacol* 2021;96:107662.

25 Lee N-R, Song E-K, Jang KY, *et al*. Prognostic impact of tumor infiltrating FOXP3 positive regulatory T cells in diffuse large B-cell lymphoma at diagnosis. *Leuk Lymphoma* 2008;49:247–56.

26 Nakayama S, Yokote T, Akioka T, *et al*. Infiltration of effector regulatory T cells predicts poor prognosis of diffuse large B-cell lymphoma, not otherwise specified. *Blood Adv* 2017;1:486–93.

27 Chang C, Wu S-Y, Kang Y-W, *et al*. High levels of regulatory T cells in blood are a poor prognostic factor in patients with diffuse large B-cell lymphoma. *Am J Clin Pathol* 2015;144:935–44.

28 Stirm K, Leary P, Bertram K, *et al*. Tumor cell-derived IL-10 promotes cell-autonomous growth and immune escape in diffuse large B-cell lymphoma. *Oncoimmunology* 2021;10:2003533.

29 Dixon KO, Schorer M, Nevin J, *et al*. Functional anti-TIGIT antibodies regulate development of autoimmunity and antitumor immunity. *J Immunol* 2018;200:3000–7.

30 Arenas-Ramirez N, Zou C, Popp S, *et al*. Improved cancer immunotherapy by a CD25-mimobody conferring selectivity to human interleukin-2. *Sci Transl Med* 2016;8:367ra166.

31 Kotecha N, Krutzik PO, Irish JM. Web-based analysis and publication of flow cytometry experiments. *Curr Protoc Cytom* 2010;Chapter 10:Unit10.

32 Levine JH, Simonds EF, Bendall SC, *et al*. Data-driven phenotypic dissection of AML reveals progenitor-like cells that correlate with prognosis. *Cell* 2015;162:184–97.

33 Frankish A, Diekhans M, Jungreis I, *et al*. GENCODE 2021. *Nucleic Acids Res* 2021;49:D916–23.

34 Hao Y, Hao S, Andersen-Nissen E, *et al*. Integrated analysis of multimodal single-cell data. *Cell* 2021;184:3573–87.

35 Li H, Handsaker B, Wysoker A, *et al*. The sequence alignment/map format and samtools. *Bioinformatics* 2009;25:2078–9.

36 Juskevicius D, Jucker D, Klingbiel D, *et al*. Mutations of CREBBP and SOCS1 are independent prognostic factors in diffuse large B cell lymphoma: mutational analysis of the SAKK 38/07 prospective clinical trial cohort. *J Hematol Oncol* 2017;10:70.

37 Hashwah H, Bertram K, Stirm K, *et al*. The IL-6 signaling complex is a critical driver, negative prognostic factor, and therapeutic target in diffuse large B-cell lymphoma. *EMBO Mol Med* 2019;11:e10576.

38 Stelling A, Hashwah H, Bertram K, *et al*. The tumor suppressive TGF-β/SMAD1/S1PR2 signaling axis is recurrently inactivated in diffuse large B-cell lymphoma. *Blood* 2018;131:2235–46.

39 Juskevicius D, Müller A, Hashwah H, *et al*. Characterization of the mutational profile of 11 diffuse large B-cell lymphoma cell lines. *Leuk Lymphoma* 2018;59:1710–6.

40 Chen X, Oppenheim JJ. Resolving the identity myth: key markers of functional CD4+Foxp3+ regulatory T cells. *Int Immunopharmacol* 2011;11:1489–96.

41 Cretney E, Kallies A, Nutt SL. Differentiation and function of FOXP3 (+) effector regulatory T cells. *Trends Immunol* 2013;34:74–80.

42 Chen B, Khodadoust MS, Liu CL, *et al*. Profiling tumor infiltrating immune cells with CIBERSORT. *Methods Mol Biol* 2018;1711:243–59.

43 Shan F, Somasundaram A, Bruno TC, *et al*. Therapeutic targeting of regulatory T cells in cancer. *Trends Cancer* 2022;8:944–61.

44 Fan MY, Low JS, Tanimine N, *et al*. Differential roles of IL-2 signaling in developing versus mature tregs. *Cell Rep* 2018;25:1204–13.

45 Yano H, Andrews LP, Workman CJ, *et al*. Intratumoral regulatory T cells: markers, subsets and their impact on anti-tumor immunity. *Immunology* 2019;157:232–47.

46 Overacre-Delgoffe AE, Chikina M, Dadey RE, *et al*. Interferon-Γ drives Treg fragility to promote anti-tumor immunity. *Cell* 2017;169:1130–1141.

47 Chuckran CA, Cillo AR, Moskovitz J, *et al*. Prevalence of intratumoral regulatory T cells expressing neuropilin-1 is associated with poorer outcomes in patients with cancer. *Science Translational Medicine* 2021;13:eabf8495.

48 Johnston RJ, Comps-Agrar L, Hackney J, *et al*. The immunoreceptor TIGIT regulates antitumor and antiviral CD8(+) T cell effector function. *Cancer Cell* 2014;26:923–37.

49 Sahin D, Arenas-Ramirez N, Rath M, *et al*. An IL-2-grafted antibody immunotherapy with potent efficacy against metastatic cancer. *Nature Communications* 2020;11:6440.

50 Salomon R, Dahan R. Next generation CD40 agonistic antibodies for cancer immunotherapy. *Frontiers in Immunology* 2022;13:940674.

51 Vonderheide RH. CD40 agonist antibodies in cancer immunotherapy. *Annu Rev Med* 2020;71:47–58.

52 van Mierlo GJD, den Boer AT, Medema JP, *et al*. CD40 stimulation leads to effective therapy of CD40(-) tumors through induction of strong systemic cytotoxic T lymphocyte immunity. *Proc Natl Acad Sci U S A* 2002;99:5561–6.

53 Vonderheide RH. The immune revolution: A case for priming, not checkpoint. *Cancer Cell* 2018;33:563–9.

54 Delgado R, Kielbassa K, Ter Burg J, *et al*. Co-stimulatory versus cell death aspects of agonistic CD40 monoclonal antibody selicrelumab in chronic lymphocytic leukemia. *Cancers* 2021;13:12.

55 Szocinski JL, Khaled AR, Hixon J, *et al*. Activation-induced cell death of aggressive histology lymphomas by CD40 stimulation: induction of bax. *Blood* 2002;100:217–23.

56 Burington B, Yue P, Shi X, *et al*. CD40 pathway activation status predicts response to CD40 therapy in diffuse large B cell lymphoma. *Science Translational Medicine* 2011;3:74ra22.

57 Ziebold JL, Hixon J, Boyd A, *et al*. Differential effects of CD40 stimulation on normal and neoplastic cell growth. *Arch Immunol Ther Exp (Warsz)* 2000;48:225–33.

58 Rydström K, Linderoth J, Nyman H, *et al*. Cd40 is a potential marker of favorable prognosis in patients with diffuse large B-cell lymphoma treated with immunochemotherapy. *Leuk Lymphoma* 2010;51:1643–8.

59 Linderoth J, Ehinger M, Jerkeman M, *et al*. Cd40 expression identifies a prognostically favourable subgroup of diffuse large B-cell lymphoma. *Leuk Lymphoma* 2007;48:1774–9.

60 Song G, Ni H, Zou L, *et al*. Expression of CD40 is a positive prognostic factor of diffuse large B-cell lymphoma treated with R-CHOP (rituximab, cyclophosphamide, doxorubicin, vincristine, and prednisone). *Onco Targets Ther* 2016;9:3799–805.